Analysis of kinetic asymmetry in a multi-cycle chemical reaction network establishes the principles for autonomous compartmentalized molecular ratchets

Emanuele Penocchio,*,†,# Ahmad Bachir,‡,# Alberto Credi,§,‖ Raymond Dean Astumian*,¶ and Giulio Ragazzon*,‡

† Department of Chemistry, Northwestern University, Evanston, IL 60208, USA

‡ Institut de Science et d'Ingégnierie Supramoléculaires (ISIS), University of Strasbourg, CNRS, 8 allée Gaspard Monge, 67000 Strasbourg, France

§ CLAN-Center for Light Activated Nanostructures, Istituto per la Sintesi Organica e la Fotoreattività, Consiglio Nazionale delle Ricerche Via Gobetti 101, 40129 Bologna, Italy

‖ Dipartimento di Chimica Industriale "Toso Montanari", Università di Bologna Viale del Risorgimento 4, 40136 Bologna, Italy

¶ Department of Physics and Astronomy, University of Maine, Orono, ME 04469, USA

# E.P. and A. B. contributed equally

KEYWORDS. Non-equilibrium systems; molecular machines; electrochemistry; chemical kinetics, endergonic processes

ABSTRACT: Kinetic asymmetry is a key parameter describing non-equilibrium chemical systems: it indicates the directionality of a chemical reaction network under steady-state, non-equilibrium conditions. So far, kinetic asymmetry has been evaluated only in networks featuring a single cycle. Here, we have investigated kinetic asymmetry in a multi-cycle system using a combined theoretical and numerical approach. Inspired by the latest experimental developments, we selected a compartmentalized redox-controlled network as a model system. We report the general analytical expression of kinetic asymmetry for multi-cycle networks, and specify it for the present system, which allows anticipating how key parameters influence directionality. We establish that compartmentalization can enable autonomous energy ratchet mechanisms, with directionality dictated by the system's thermodynamics. Kinetic simulations confirm analytical findings and illustrate the interplay between diffusion, chemical, and electrochemical processes. The presented treatment is general, as the same procedure can be used to assess kinetic asymmetry in other multi-cycle networks, facilitating the realization of endergonic processes across domains.

INTRODUCTION

Operating away from equilibrium is a key feature of life and holds great promise for developing chemical systems with advanced functionalities.[1–4] Ultimately, a non-equilibrium chemical system can be described as a chemical reaction network exchanging energy with its surroundings.[5–8] When the reactions of the network can occur repeatedly under constant environmental conditions in the presence of a continuous energy supply, the system is said to be autonomous.[9,10] A key property to describe the dynamics of a such a network is kinetic asymmetry,[11,12] which reports on the directionality of the chemical reaction network at the steady state. This piece of information has been used to rationalize the operation of chemically driven autonomous molecular motors,[12–18] non-equilibrium self-assembly,[19–22] chemotaxis,[23,24] non-reciprocal interactions,[25] as well as several other processes requiring an energy input to occur, i.e., endergonic.[26,27]

So far, the description of kinetic asymmetry in chemical reaction networks has been limited to cyclic networks having a single cycle, i.e., networks where the relevant cyclic sequence of reactions involves all intermediates present in the system.[12,19,28–32] In these networks, kinetic asymmetry can be expressed as the product of the reactions' rates along the cycle in one direction over the product of the rates in the opposite direction.[26] This simple description breaks down when only some of the species participate in the relevant reaction cycle, which is the subject of this work (Figure 1). In this situation, multiple cycles can contribute to kinetic asymmetry.

Multi-cycle chemical reaction networks are fairly easy to realize experimentally. A simple strategy is to consider a system having two switchable properties (e.g., redox state and conformation), resulting in a square reaction network as the one in Figure 1a, and add the possibility to diffuse between two spatially different locations – or compartments; the resulting network corresponds to the one in Figure 1b. We decided to investigate this network because it represents the logical extension of widely explored square schemes. The same type of network can also describe a recent experimental example, where redox process and a self-

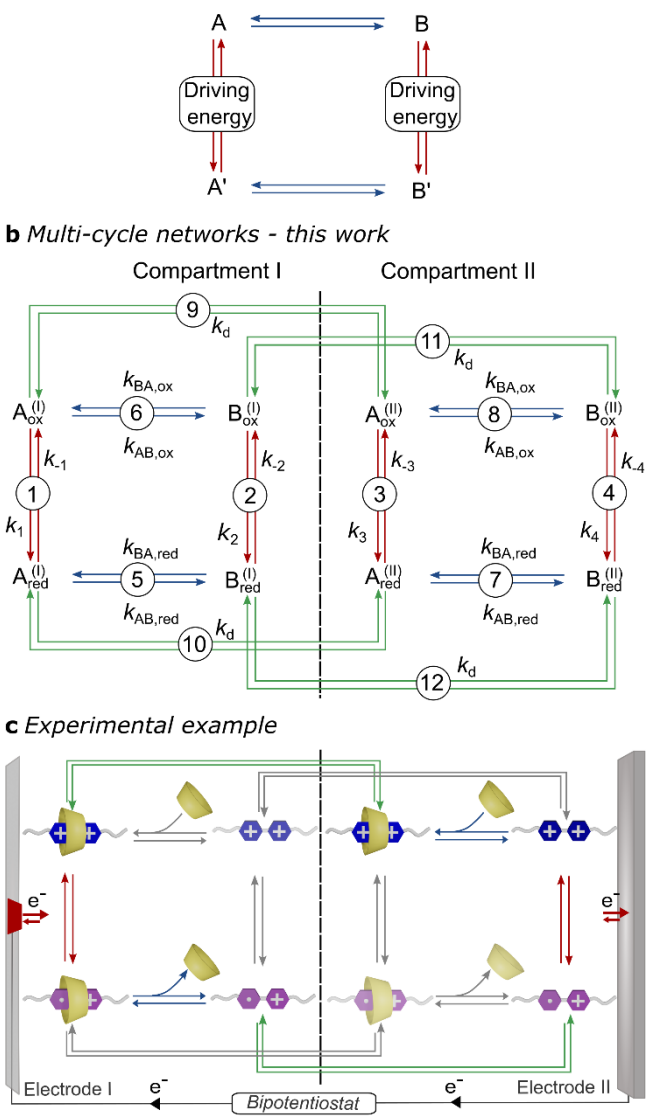

Figure 1. Comparison between (a) a 4-species mono-cycle chemical reaction network and (b) the 8-species multi-cycle chemical reaction network discussed in this work, obtained upon forming two compartments divided by a permeable membrane (dashed). Without loss of generality, we identify reactions as proceeding in the positive direction when going from ox to red in the case of redox reactions, from B to A in the case of chemical reactions, and from compartment I to compartment II in case of diffusion processes. (c) Illustration of an experimental example that can be rationalized using the present approach, comprising a redox-active host-guest system; self-assembly and redox reactions would form a square reaction network, in the vicinity of each electrode; the shaded states and reactions are less relevant than others experimenatally. In all panels, reactions are color-coded, with red steps exchanging energy with the source, blue steps indicating chemical reactions, and green steps representing diffusion across the permeable barrier.

assembly reaction were combined with diffusion to obtain an autonomous system powered by electrical energy.[33] As sketched in Figure 1c, the authors operated the redox-switchable host-guest system between the electrodes of a scanning electrochemical microscope, which allowed the simultaneous promotion of oxidation and reduction at two independently controlled electrodes. This condition is gaining mounting attention and has already demonstrated its potential in surface and material science.[34,35] In the work focused on autonomous operation, the authors used kinetic simulations to support the idea that the system's operation was predominantly controlled by an autonomous energy ratchet mechanism, i.e., a mechanism where directionality is dictated solely by the thermodynamic stability of intermediates.[33,36] Such an autonomous operation mechanism was previously described in detail exclusively in relation to light-driven systems,[37–39] and, as a result, the theoretical basis for such a mechanism remains unexplored in relation to ground-state reactivity.[40]

Here, we present the treatment of kinetic asymmetry in an epitomic multi-cycle network. In particular, we focused on a redox-powered network, mapping closely the one underlying the recently reported autonomous electrically driven system, to investigate the origin of its somewhat unconventional ratchet mechanism. We identify a regime compatible with experimental observations where directionality is solely controlled by thermodynamic features of the system while the kinetics of diffusion processes should be intermediate between other processes, thus establishing the principles for autonomous compartmentalized molecular energy ratchets. Analytical results are validated by numerical simulations, which we also use to show that diffusion rates can be tuned to implement an information ratchet mechanism within the same system. Although we focus on a specific case study, our approach is general and can be used to analyze kinetic asymmetry in virtually any multi-cycle chemical reaction network.

Finally, we stress that we kept mathematical treatments to a minimum in the main text. Interested readers can refer to the SI for the full step-by-step analysis.

RESULTS & DISCUSSION

Model system. The system is controlled by two electrodes, and the two compartments model the proximity to them. In compartment I, species are close to electrode I, which is kept at potential E_I. In compartment II, species are close to electrode II. Within each compartment, the concentrations are considered uniform. Species can diffuse between the two compartments according to first-order processes controlled by diffusion constants k_d (reactions 9-12).

In each of the two compartments, the same 4-species square reaction network is present, resulting from orthogonal redox and chemical processes. Species **A** and **B** can interconvert thermally via reactions 5-8. The oxidized species $\mathbf{A}_{ox}$ and $\mathbf{B}_{ox}$ are converted to their reduced counterparts $\mathbf{A}_{red}$ and $\mathbf{B}_{red}$, via electrochemical reactions 1-4 occurring at the two electrodes. The thermodynamic properties of the reactions forming a square cycle are related by the microscopic reversibility constraint:

$$K_{ox}K_{red}^{-1} = e^{(F/RT)(E_B^0 - E_A^0)} = e^{(F/RT)\Delta E^0} \qquad (1)$$

where Ks are the equilibrium constants of the chemical reactions, defined as $K = k_{BA}/k_{AB}$, F and R the Faraday and the

gas constants, respectively, T the temperature, and E^0s are the standard redox potentials of species **A** and **B**.

The rate of redox processes is described by Butler-Volmer kinetics, the standard approach for describing heterogeneous electron transfer.[41] In essence, the equilibrium populations of $\mathbf{A}_{ox}$ and $\mathbf{A}_{red}$ (and analogously $\mathbf{B}_{ox}$, $\mathbf{B}_{red}$) in each compartment depend on the standard redox potential of this redox couple (E_A^0) and the potential applied to the electrode, which therefore can be used to control their relative thermodynamic stability within a compartment. When the potentials of the two electrodes differ, an electrochemical potential gradient $\Delta E = E_{II} - E_I$ is established between the two compartments, and energy is available to drive the system away from equilibrium.

We note that the investigated model consists of only unimolecular chemical reactions, but since kinetic asymmetry is a steady-state property, our findings also extend to systems that feature bimolecular self-assembly reactions. Indeed, concentrations are constant at the steady-state, which allows describing bimolecular self-assembly reactions as pseudo-first-order processes. This consideration is relevant also to the experimental system that inspired this work, which comprises self-assembly steps.[33] The parallel of our model with the experimental setup is further reinforced by the absence of convection and migration phenomena, which are routinely excluded under the relevant experimental conditions.

General analytical treatment. From a chemical perspective, it is interesting to understand when the transport of electrons can influence other reactions, in principle unrelated to the redox process. In the present case, it is a matter of understanding if the chemical reactions 5-8 interconverting A and B can use some of the energy provided by the electric current via redox reactions 1-4 to depart from equilibrium and generate a directed net flux across the chemical reaction network. At the level of a chemical reaction network, this type of energy transduction can take place once there is a sequence of steps that makes two different processes happen simultaneously (not in sequence). For example, here the sequence of reactions 1→–5→12→–4→–11 (see the caption of Figure 1b for the notation and sign convention) transfers one electron from electrode I to electrode II, and simultaneously converts $\mathbf{A}_{ox}$ in $\mathbf{B}_{ox}$. In line with literature on molecular machines,[10,26,27,42] we refer to this condition as the *coupling* of the redox reactions to the chemical steps, while being aware that the same term is used also with less technically stringent meaning in the broader chemical literature. Promoting coupled chemical reactions is the outcome of an operating ratchet mechanism.[26,27] In practice, an operative ratchet mechanism would imply that the conversion of **A** into **B** happens preferentially in one redox state, say, in the reduced state (i.e., a net flux $\mathbf{A}_{red} \rightarrow \mathbf{B}_{red}$, independently of the compartment) and the conversion of **B** into **A** occurs in the other redox state, say, in the oxidized state (i.e., a net flux $\mathbf{B}_{ox} \rightarrow \mathbf{A}_{ox}$). If this were the case, then cycling through the network according to the sequence $\boldsymbol{S}$: $\mathbf{A}_{ox} \rightarrow \mathbf{A}_{red} \rightarrow \mathbf{B}_{red} \rightarrow \mathbf{B}_{ox} \rightarrow \mathbf{A}_{ox}$ would have a different probability than the reversed sequence: $\boldsymbol{S}^{-1}$: $\mathbf{A}_{ox} \leftarrow \mathbf{A}_{red} \leftarrow \mathbf{B}_{red} \leftarrow \mathbf{B}_{ox} \leftarrow \mathbf{A}_{ox}$. Therefore, sequence $\boldsymbol{S}$ describes the coupling of the redox reactions to the chemical steps. In this particular network, sequence $\boldsymbol{S}$ is the only coupling that can arise; more than one coupled sequence may be present in more complex systems.

At the steady state, the overall directional bias for the sequence $\boldsymbol{S}$, namely, the kinetic asymmetry of the chemical reaction network, can be quantified as the ratio between the (average) frequencies at which sequences $\boldsymbol{S}$ and $\boldsymbol{S}^{-1}$ are traveled. Such a ratio is typically called "ratcheting constant", K_r, or "directionality", r_0. As an equilibrium constant quantifies the bias in the concentrations of reactants and products at equilibrium, K_r is a non-equilibrium constant quantifying the kinetic preference for traveling the sequence $\boldsymbol{S}$ with respect to $\boldsymbol{S}^{-1}$. In particular, $K_r > 1$ denotes a preference for sequence $\boldsymbol{S}$, $K_r < 1$ denotes a preference for sequence $\boldsymbol{S}^{-1}$, and $K_r = 1$ denotes the absence of a kinetic bias in the system, a condition often referred to as "kinetic symmetry" corresponding, in this case, to the chemical reactions not being coupled to the inter-electrode current. Mathematically, K_r can be computed by dividing the sum of the frequencies (j) of all the cycles realizing the sequence $\boldsymbol{S}$ for the sum of the frequencies of all the cycles realizing $\boldsymbol{S}^{-1}$. Therefore, to quantify kinetic asymmetry, we need to identify all the cycles that contribute to $\boldsymbol{S}$ and $\boldsymbol{S}^{-1}$, which can be of three types, differing in how they are coupled to the energy source.

Slip cycles,[28] $\mathcal{R}$, realize sequence $\boldsymbol{S}$ without moving any net number of electrons between the electrodes. An example is the counterclockwise cycle 1→–5→–2→6. These cycles are not associated with a net exchange of energy, therefore their microscopic reverse cycles (such as clockwise –6→2→5→–1) are equally likely and thus slip cycles do not give a net contribution to directionality.

The forward cycles, $\mathcal{F}$, are those cycles realizing the sequence $\boldsymbol{S}$ and concomitantly moving one electron from electrode I to electrode II. For example, the counterclockwise cycle 1→–5→12→–4→8→–9 is a forward cycle. The frequency with which this cycle is traveled with respect to its microscopic reverse (clockwise 9→–8→4→–12→5→–1) is controlled by the electrochemical potential gradient. In particular, forward cycles are $e^{(F/RT)\Delta E}$ times faster than the corresponding microscopic reverses. In the absence of a gradient ($\Delta E = 0$), no preferred directionality emerges, while forward cycles directly contribute to directionality in the presence of a gradient.

The backward cycles, $\mathcal{B}$, realize the sequence $\boldsymbol{S}^{-1}$ and concomitantly move one electron from electrode I to electrode II. For example, the cycle 2→5→10→–3→–8→–11 is a backward cycle. As in the case of forward cycles, a net electron current is associated with the cycle, and a contribution to directionality can arise in the presence of a gradient.

After some algebraic passages (see SI section 2.1) K_r can be expressed as:

$$K_r = \frac{q + e^{-(F/RT)\Delta E} + \Gamma}{q e^{-(F/RT)\Delta E} + 1 + \Gamma} \qquad (2)$$

with

$$q = \frac{\sum_i j_{F_i}}{\sum_i j_{B_i}} \qquad (3)$$

$$\Gamma = \frac{\sum_i j_{R_i}}{\sum_i j_{B_i}} \qquad (4)$$

where $j\chi_i$ denotes the frequency of cycle χ_i and summations are intended to run over all the forward, backward, and slip cycles.

This expression of K_r – derived in the context of electrochemical systems – takes the exact same form[28,40,43] that characterizes catalysis-driven systems, where the chemical potential gradient of the catalyzed reaction plays the role of ΔE, thus offering a unified treatment of ratchet mechanisms in the ground state. Equation 2 contains only three system-specific parameters: ΔE, q, and Γ, which are solely responsible of directionality. Their meaning is intuitive: ΔE reflects the energy available to drive the non-equilibrium process; q compares the forward and backward cycles (promoting $\boldsymbol{S}$ or $\boldsymbol{S}^{-1}$, respectively), thus reporting on the overall kinetic bias. Γ reports on the relative weight of slip cycles, which do not contribute directly to directionality. We can use this reasoning to interpret a few mathematical relations derived from Equation 2 (see the SI section 2.1 for proof). When $\Delta E = 0$, the numerator and denominator become equal, and $K_r = 1$, therefore no directionality can emerge, reiterating the necessity of an energy source. Directionality is also suppressed when Γ – appearing both in the numerator and denominator – is large. The larger Γ, the closer to 1 K_r will be, meaning that the slip cycles dominate, and the inter-electrode current is only weakly coupled to the chemical reactions. In the limit of $\Gamma \to 0$, known as the complete coupling or strong coupling regime,[40] the effectiveness of the ratchet mechanism is maximized, as chemical reactions will almost always happen concurrently to electron transport. Focusing on the effect of q, when $\Delta E > 0$, K_r will be greater (smaller) than one if $q >$ (<)1. On the contrary, when $\Delta E < 0$, K_r will be greater (smaller) than one if $q <$ (>)1. In the context of catalysis-driven systems, the overall kinetic bias q is related to the difference in the transitions states' free energy between the forward and backward cycles and is sometimes called the "Curtin-Hammett asymmetry factor" (denoted $F_{C\text{-}H}$) in light of its connections with kinetic resolution.[43] Here, the kinetic bias is intrinsically related to the thermodynamic bias via the Butler-Volmer equation, and its interplay with compartmentalization. In redox reactions, the interplay between kinetics and thermodynamics may also be non-linear, as occurring for example in the reactions described by Marcus theory of electron transfer; we note that implementing such reaction kinetics would afford non-equilibrium systems characterized by a negative differential response.[44]

Diagram method for cycles' frequencies. The analysis presented so far is valid for any chemical reaction network controlled by electrochemical reactions occurring at two electrodes. Now, we detail how the general treatment applies to the specific network of Figure 1b.

To compute q, we need to identify all cycles of type $\boldsymbol{\mathcal{F}}$ and $\boldsymbol{\mathcal{B}}$ and compute the corresponding-frequencies. The present network has four $\boldsymbol{\mathcal{F}}$ and four $\boldsymbol{\mathcal{B}}$ cycles, illustrated in Figure 2. The procedure used to calculate cycles' frequencies is based on diagram method derived from graph theory.[45–47] In particular, we adopted the notation illustrated in Ref.[48] We anticipate that the frequency associated to a given cycle χ – as well as any other cycle considered here – can be expressed in the following form:

$$j_X = \frac{\Pi_X \Sigma_X}{N} \qquad (5)$$

N is a normalizing constant common to all the cycles; it simplifies out when computing q, and its explicit computation is therefore not necessary here. The term Π_χ is the product of all the rate constants involved in the cycle. Heuristically, it can be thought of as a measure of how fast the cycle χ gets traveled on average; the same terms appear also in the computation of kinetic asymmetry in mono-cycle networks.

The Σ_χ term only appears in multi-cycle networks and can be thought of as a factor expressing the probability of entering cycle χ. Mathematically, Σ_χ is the sum of the contributions from all the so-called "rooted spanning trees"[47] of cycle χ. A rooted spanning tree is a sequence of reactions entering the cycle starting from all the species not included in the cycle (without forming new cycles).

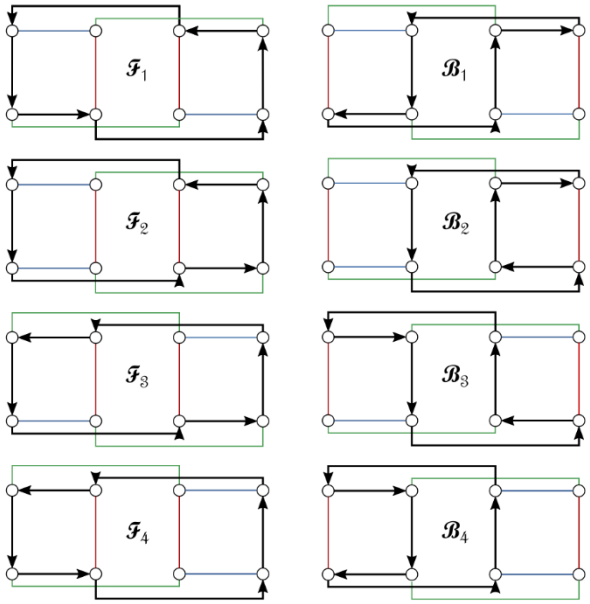

Figure 2. Schematic representation of all possible cycles (black arrows), that move one electron from compartment I (left) to compartment II (right) while realizing the sequence $\boldsymbol{S}$ (forward cycles, $\boldsymbol{\mathcal{F}}_i$) and the sequence $\boldsymbol{S}^{-1}$ (backward cycles, $\boldsymbol{\mathcal{B}}_i$). The network species, reactions, and color-coding coincide with those reported in Figure 1b., e.g., the top left species is $\mathbf{A}_{ox}{}^{(c)}$, and the leftmost vertical connection corresponds to reaction 1.

Cycle $\mathcal{F}_1$ corresponds to the most important cycle in the reference experimental case (cf. Figure 1c and 2). Therefore, we take it as an example and depict all its rooted spanning trees in Figure 3. The contribution to Σ_{F1} of each spanning tree is the product of the rate constants involved as shown in Figure 3, Σ_{F1} being the sum of the contributions from all the spanning trees. The detailed mathematical expression of terms Π_χ and Σ_χ for all the relevant cycles are reported in the SI.

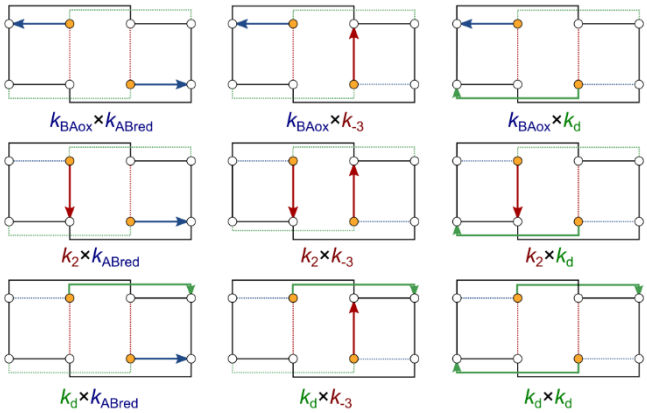

Figure 3. Rooted spanning trees for cycle $\mathcal{F}_1$, the corresponding contributions to Σ_{F1} are indicated below their graphical representation. Cycle $\mathcal{F}_1$ is reported in black, the species not included in the cycle are indicated in orange. The network species, reactions, and color-coding coincide with those reported in Figure 1b and 2.

Autonomous energy ratchet operation. From now on, with the intent of seeking purely energy ratchet effects, we purposely exclude kinetic biases by considering all species as having the same diffusion constant k_d and charge-transfer coefficient, a realistic regime for the experimental systems that inspired this work. (see SI section 1).[33]

Computing all Π_χ terms reveals that all Π_F and Π_B terms are equal. This finding can be used (see SI section 2.2) to simplify the general expression of q into the following system-specific form:

$$q = \frac{\Sigma_{F_1}+\Sigma_{F_2}+\Sigma_{F_3}+\Sigma_{F_4}}{\Sigma_{B_1}+\Sigma_{B_2}+\Sigma_{B_3}+\Sigma_{B_4}} \qquad (6)$$

This expression contains only spanning tree terms – peculiar to multi-cycle systems – which are evidently essential in controlling directionality. In particular, the sums at the numerator and denominator take the following expressions:

$$\begin{aligned}&\Sigma_{F_1}+\Sigma_{F_2}+\Sigma_{F_3}+\Sigma_{F_4} = \\ &= \left(e^{(F/2RT)\Delta E}e^{(F/2RT)\Delta E^0}+1\right)\times C_1 + \\ &+\left(e^{(F/RT)\Delta E}e^{(F/RT)\Delta E^0}+1\right)\times C_2 + C_3 \end{aligned} \qquad (7)$$

$$\begin{aligned}&\Sigma_{B_1}+\Sigma_{B_2}+\Sigma_{B_3}+\Sigma_{B_4} = \\ &= \left(e^{(F/2RT)\Delta E}+e^{(F/2RT)\Delta E^0}\right)\times C_1 + \\ &+\left(e^{(F/RT)\Delta E}+e^{(F/RT)\Delta E^0}\right)\times C_2 + C_3 \end{aligned} \qquad (8)$$

where parameters $C_{1\text{-}3}$ are functions of the rate constants and electrochemical potentials characterizing the network, for example:

$$\begin{aligned}&C_3 = \left(k_{BA,ox}+k_{AB,ox}+2k_d\right)\times \\ &\times\left(k_{BA,red}+k_{AB,red}+2k_d\right)\end{aligned} \qquad (9)$$

Where $k_{AB,ox(red)}$ is the rate constant for the formation of **B** in the oxidized (reduced state), and $k_{BA,ox(red)}$ its microscopic reverse (see Figure 1b). The expressions of parameter C_1 and C_2 are reported in the SI.

Given the final form of Equations 7 and 8, it can be demonstrated (see SI section 2.2 for the proof) that ratio q in Equation 6 will be larger or smaller than one depending on the sign of $\Delta E\times\Delta E^0$, thus the electrochemical potential gradient ΔE and the difference standard redox potentials ΔE^0 control q. Specifically, q is > 1 if $\Delta E\times\Delta E^0$ >1, and q is < 1 if $\Delta E\times\Delta E^0$ <1. Since ΔE and ΔE^0 control q, it may seem that they both control directionality, K_r, expressed by Equation 2. However, since Equation 2 contains q and ΔE both at the numerator and the denominator, the sign of ΔE does not influence directionality. As a result, ΔE^0 is the sole responsible of directionality in the investigated network. ΔE^0 is intrinsic to the system at study, and inherently related to the equilibrium constant of the chemical reactions by the microscopic reversibility constraint reported in Equation 1. At any given potential difference other than zero between the electrodes, directionality is dictated by thermodynamic features, a hallmark of energy ratchet mechanisms. Yet, ΔE can be controlled externally simply by changing electrode potentials. As a result, both the driving force and directionality can be modulated at will, which is considerably harder – and sometimes even practically impossible – to achieve in systems powered by chemical energy or light.

Additional insights are offered by the expression of parameter C_3 (Equation 9), which is the only term contributing to q that is independent from ΔE and ΔE^0. If diffusion is much faster than chemical reactions, C_3 dominates the ratio in Equation 6, and directionality vanishes. Therefore, chemical reactions should be faster than diffusion for an optimal q value. However, when diffusion is too slow, slip cycles become dominant (e.g. the sequence 1→–5→–2→6, entirely occurring in the cathodic compartment, *vide supra*). Mathematically, this is reflected in larger values of Γ, which suppress directionality according to Equation 2.

Non-equilibrium species concentration. The occurrence of a non-equilibrium steady-state – featuring directional reaction fluxes – implies a concentration imbalance with respect to equilibrium. Comparing concentrations in the presence and the absence of energy inputs is often a viable experimental measure to probe the coupling's effectiveness. In this particular case, it is insightful to compare the total amounts of species **A** and **B** in the oxidized and reduced state. If the chemical reactions were at equilibrium, those ratios would equal K_{ox} and K_{red}, respectively. Therefore, values different from the corresponding equilibrium constant are signatures of the coupling. We can express these ratios by using the same analytical treatment we used

to express K_r. After some algebraic passages (see SI Section 2.3), we find

$$\frac{[A_{red}^{(I)}]+[A_{red}^{(II)}]}{[B_{red}^{(I)}]+[B_{red}^{(II)}]} = K_{red} \times \left\{\frac{q+e^{-(F/RT)\Delta E}+\psi_{red}}{qe^{-(F/RT)\Delta E}+1+\psi_{red}}\right\} \quad (10)$$

$$\frac{[A_{ox}^{(I)}]+[A_{ox}^{(II)}]}{[B_{ox}^{(I)}]+[B_{ox}^{(II)}]} = K_{ox} \times \left\{\frac{qe^{-(F/RT)\Delta E}+1+\psi_{ox}}{q+e^{-(F/RT)\Delta E}+\psi_{ox}}\right\} \quad (11)$$

The above Equations show that the same parameters controlling directionality also control concentration ratios. In fact, the terms in brackets are closely related to K_r in Equation 2. When K_r = 1, equivalent to ΔE = 0 and/or ΔE° = 0 (leading to q=1, see discussion in the previous Section), the terms in brackets are also unitary, leading to no concentration imbalance with respect to equilibrium. When K_r > 1, equivalent to ΔE ≠ 0 and ΔE° > 0 (leading to q > 1), chemical reactions depart from equilibrium favoring A_{red} and B_{ox} species over $\mathbf{B}_{red}$ and $\mathbf{A}_{ox}$, respectively. When K_r < 1, equivalent to ΔE ≠ 0 and ΔE° < 0 (leading to q < 1), nonequilibrium conditions favor $\mathbf{B}_{red}$ and $\mathbf{A}_{ox}$ species over $\mathbf{A}_{red}$ and $\mathbf{B}_{ox}$, respectively. The two new parameters appearing in Equations 10 and 11, ψ_{ox} and ψ_{red}, are analogous to Γ in Equation 2 in that they report on the effectiveness of the ratchet mechanism (see SI section 2.3 for their analytical expressions). Namely, for large ψs, nonequilibrium ratios will remain close to the corresponding equilibrium ratios, making the coupling poor.

Equations 10 and 11 are instances of the nonequilibrium pumping equality,[49,50] a general result in trajectory thermodynamics, relating the steady-state chemical potential difference between two species to the exponential of the excess work exchanged with the environment kinetically weighted and averaged over all trajectories between those two species. The latter quantity is not straightforward to compute explicitly in complicated networks. Here, we could provide an analytical expression by leveraging graph-theoretical techniques, as detailed in the SI. The ratcheting constant K_r and the nonequilibrium pumping equality epitomize the fundamental role of kinetic asymmetry, here reflected in the parameter q, for harnessing energy and realizing functions out-of-equilibrium.

Numerical investigation. To investigate the impact of our findings on a plausible system, we assigned reasonable values to the parameters characterizing the investigated network and performed numerical simulations to investigate the effect of network parameters and confirm the analytical predictions. Chemical reactions were imposed having a rate in the order of 1-100 s^{-1}, somewhat slower than typical NMR timescales. A reduction potential of -0.2 V was selected for species **A**, which is close to the reduction potential of the viologen species involved in the experimental study which inspired this work.[33] Since all reactions involved follow a first-order kinetic, the model system is insensitive to the total species concentration. Significantly, the diffusion constants k_d differ from typical diffusion values, because here they report on the propensity of species to change compartment, and not the actual propensity to move in space. Indeed, the dimension of k_d is $time^{-1}$, while diffusion coefficients are expressed in $length^2 \times time^{-1}$. In most cases, under the simulation conditions electrode I serves as a cathode, promoting species reduction, while electrode II serves as an anode, promoting oxidation.

The results obtained from exploring the dependence of chemical reactions' fluxes (net conversion from B to A) on electrode potentials, equilibrium constants, and diffusion constants are reported in Figure 4a-d.

When both electrodes have the same potential (–0.2 V) there are no reaction fluxes (i.e., the system reaches equilibrium). On the contrary, when the E_{II} becomes more positive, directional reaction fluxes emerge, which reach a plateau slightly above the E_B^0. If the E_{II} becomes more negative than E_I, lower than the cathode, the fluxes maintain their sign (Figure 4a), in line with the general analytical treatment presented above identifying ΔE^0 as the sole determinator of directionality. Yet, the magnitude of fluxes is significantly different, with a ca. 10^6-times difference between the two plateaus observed. Modulation of the equilibrium constants affords results in line with the analytical findings, reporting a current inversion around equilibrium constant equality (Figure 4b). In this case, the fluxes' magnitude is symmetrical with respect to the energetic imbalance imposed (see Figure S2c for the logarithmic plot). The observed behavior is reminiscent of Tafel plots, which relate current and overpotential: this observation is less surprising when realizing that changing the equilibrium constant also changes the redox potential – to respect the detailed balance constraint in

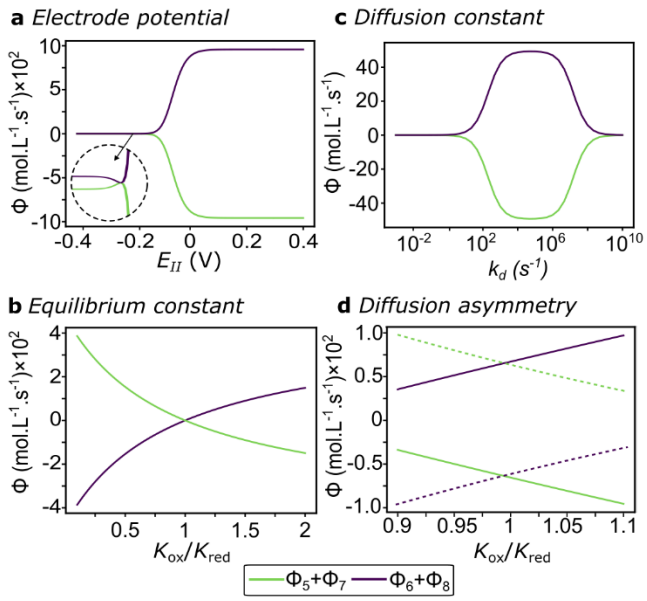

Figure 4. Dependence of reaction fluxes ($\Phi_5 = k_{BA,red}$ [$\mathbf{B}_{red}^{(I)}$] - $k_{AB,red}$ [$\mathbf{A}_{red}^{(I)}$]; $\Phi_6 = k_{BA,ox}$ [$\mathbf{B}_{ox}^{(I)}$] - $k_{AB,ox}$ [$\mathbf{A}_{ox}^{(I)}$]; $\Phi_7 = k_{BA,red}$ [$\mathbf{B}_{red}^{(II)}$] - $k_{AB,red}$ [$\mathbf{A}_{red}^{(II)}$]; $\Phi_8 = k_{BA,ox}$ [$\mathbf{B}_{ox}^{(II)}$] - $k_{AB,ox}$ [$\mathbf{A}_{ox}^{(II)}$]) on model parameters: a) electrode potential; b) equilibrium constants of chemical reactions; c) diffusion coefficient and d) diffusion asymmetry, obtained slowing down 1000 times species **B** (full lines) or species **A** (dashed lines), and observed in proximity of K_{ox}/K_{red}.= 1, where fluxes are zero in the absence of diffusion asymmetry. According to the above equations, a positive flux indicates that the conversion from **B** to **A** is dominant over the opposite process. Details of numerical simulation are given in the text and SI section 3.

Equation 1 – thus the overpotential. Since fluxes and concentration imbalances are directly related, the same numerical results also corroborate the analytical findings discussing non-equilibrium concentrations. (see Figure S5 for the explicit numerical verification of Equations 10 and 11).

Changing the diffusion coefficient over twelve orders of magnitude revealed the bell-shaped curve predicted by the network-specific analytical treatment (Figure 4c). The onset of fluxes occurs close to $k_d = 1$, with fluxes reaching a plateau above $k_d = 10^2$. These values coincide with the rate constants associated with chemical reactions, the slowest processes in the network. Instead, the fluxes vanish around $k_d = 10^6$, which is comparable with rates of redox processes, the fastest reactions in the network. Therefore, chemical and electrochemical parameters control the shape of the bell curve. This interpretation was corroborated by simulations in which the shape of the bell was selectively modulated by changing chemical and electrochemical parameters. For example, slowing all the chemical reactions by one order of magnitude shifts only the low-diffusion flux onset, while speeding up all the redox processes analogously shifted only the high-diffusion flux onset (see Figure S3). A similar reasoning might apply to the bell-shaped profile predicted for the turnover frequency associated to heterogeneous catalysis occurring under alternating conditions.[51] In the present case, the region characterized by high diffusion constants and low fluxes seems however hard to investigate experimentally, as it falls close to the ns time scale. Interestingly, simulations performed keeping both electrodes at negative potentials (Figure S4a-c) illustrated that fluxes are also observed when both electrodes are kept at potentials lower than the redox potential of both species involved. Since the occurrence of a directional flux implies the absorption of energy from a source, this phenomenon might be used to harvest energy from any potential difference, acquiring a broader significance.

Finally, we took advantage of numerical simulation to investigate the effect of diffusion asymmetry.[24] To this aim, we imposed a different diffusion constant for species **A** with respect to species **B**. In this case, even in the absence of a thermodynamic bias a directional current was observed, which was reversed when the diffusion asymmetry was reversed (Figure 4d). On the contrary, differentiating the rates of chemical reactions did not produce analogous effects (Figure S4d-e). These simulations indicate that diffusion asymmetry can give rise to a pure information ratchet effect and imply that in compartmentalized systems energy and information ratchet effects can coexist.[26,52] Indeed, diffusion asymmetry was present in the experimental example discussed above,[33] however the difference in diffusion coefficients was modest (1.5 times) and directionality remained dictated by thermodynamic stabilities. In line with experimental evidence and simulations, systems involving supramolecular polymers[22] or metabolons[53] would more easily present properties stemming from diffusion asymmetry, compared to small-molecule systems. Overall, the numerical simulations corroborated analytical results, and allowed us to gain additional insights, specifically on the factors controlling the bell-shaped profile of fluxes vs diffusion constant, and the additional opportunities opened by diffusion asymmetry, whose detailed investigation goes beyond the scope of the present article.

CONCLUSION

This work unlocks the description of kinetic asymmetry in multi-cycle networks. The analytical treatment leading to Equation 2 and the diagrammatic method to find cycles' frequencies are general and can be applied[54] to any multi-cycle chemical reaction network. Here, we focused on a compartmentalized system powered by redox reactions and leveraged it to establish the theoretical basis for autonomous energy ratchet mechanisms enabled by compartmentalization. The characteristic features of this broadly applicable ratchet mechanisms are the following: (*i*) when $\Delta E = 0$ (no driving) or when $\Delta E^0 = 0$ (i.e., $K_{ox} = K_{red}$), no energy ratchet mechanism is active and chemical steps are predicted to be at equilibrium (no net current); (*ii*) having $\Delta E \neq 0$ is not sufficient to impart directionality in the network, as an overall kinetic bias ($q \neq 1$) is also necessary; the sequence S is traveled preferentially in the forward (backward) direction if $\Delta E^0 > (<) 0$, namely $K_{ox}/K_{red} > (<) 1$; (*iii*) fast diffusion is predicted to hamper directionality and reduce the current across the chemical reactions; slow diffusion is predicted to maintain directionality but reducing currents as well by slowing down cycles' fluxes. On top of anticipating reaction fluxes, the same treatement has been used to predict non-equilibrium concentrations, an often experimentally accessible parameter. This prediction was obtained by retrieving the non-equilibrium pumping equality by leveraging graph-theoretical techniques. The analytical findings have been corroborated by numerical simulations, which also revealed the processes controlling the bell-shape profile features and indicated that energy and information ratchet effects can coexist in compartmentalized systems, for example in the presence of diffusion asymmetry. Our findings have implications for the development of endergonic processes across domains of chemistry, from metabolism,[55] to redox-active systems,[56–59] to molecular machines,[60,61] to chemotaxis and compartmentalization,[62–64] also in a prebiotic environment,[65–67] as well as the development of soft materials,[68,69] thermo-electrochemical cells,[70,71] sensing,[72] and surface pattering under non-equilibrium conditions.[73]

ASSOCIATED CONTENT

Supporting Information. Detailed mathematical derivations and details of kinetic modeling.

AUTHOR INFORMATION

Corresponding Authors

* Giulio Ragazzon, email: ragazzon@unistra.fr
* Raymond Dean Astumian, email: astumian@maine.edu
* Emanuele Penocchio, email: . emanuele.penocchio@northwestern.edu

Author Contributions

# E.P. and A. B. contributed equally.

ACKNOWLEDGMENT

This work was supported by the Interdisciplinary Thematic Institute ITI-CSC via the IdEx Unistra (ANR-10-IDEX-0002) within the program Investissement d'Avenir and the European Research Council (ERC-2021-StG 101041933 – KI-NET to G.R.). A.B. thanks the CSC Graduate School funded by the French National Research Agency (CSC-IGS ANR-17-EURE-0016) and the Region Grand Est (ACTION 15 SESRI – Volet 2, 22-DOC-065) for a PhD fellowship. The authors would like to thank Benjamin M. W. Roberts and Massimo Bilancioni for insightful comments.

REFERENCES

[1] E. Mattia, S. Otto. Supramolecular systems chemistry, *Nat. Nanotechnol.* **2015**, *10*, 111–119.

[2] B. A. Grzybowski, W. T. S. Huck. The nanotechnology of life-inspired systems, *Nat. Nanotechnol.* **2016**, *11*, 585–592.

[3] A. Walther. Viewpoint: From Responsive to Adaptive and Interactive Materials and Materials Systems: A Roadmap, *Adv. Mater.* **2019**, 1905111.

[4] C. Kaspar, B. J. Ravoo, W. G. van der Wiel, S. V. Wegner, W. H. P. Pernice. The rise of intelligent matter, *Nature* **2021**, *594*, 345–355.

[5] H. Qian, D. A. Beard. Thermodynamics of stoichiometric biochemical networks in living systems far from equilibrium, *Biophys. Chem.* **2005**, *114*, 213–220.

[6] T. T. Le Saux, R. R. Plasson, L. L. Jullien. Energy propagation throughout chemical networks, *Chem. Commun.* **2014**, *50*, 6189–6195.

[7] R. Rao, M. Esposito. Nonequilibrium thermodynamics of chemical reaction networks: Wisdom from stochastic thermodynamics, *Phys. Rev. X* **2016**, *6*, 1–23.

[8] A. I. Brown, D. A. Sivak. Theory of Nonequilibrium Free Energy Transduction by Molecular Machines, *Chem. Rev.* **2020**, *120*, 434–459.

[9] E. R. Kay, D. A. Leigh. Rise of the Molecular Machines, *Angew. Chem. Int. Ed.* **2015**, *54*, 10080–10088.

[10] M. Baroncini, S. Silvi, A. Credi. Photo- And Redox-Driven Artificial Molecular Motors, *Chem. Rev.* **2020**, *120*, 200–268.

[11] R. D. Astumian, P. B. Chock, T. Y. Tsong, H. V Westerhoff. Effects of oscillations and energy-driven fluctuations on the dynamics of enzyme catalysis and free-energy transduction, *Phys. Rev. A* **1989**, *39*, 6416–6435.

[12] R. D. Astumian. Kinetic asymmetry allows macromolecular catalysts to drive an information ratchet, *Nat. Commun.* **2019**, *10*, 3837.

[13] E. R. Kay, D. A. Leigh, F. Zerbetto. Synthetic molecular motors and mechanical machines., *Angew. Chem. Int. Ed.* **2007**, *46*, 72–191.

[14] M. R. Wilson, J. Solà, A. Carlone, S. M. Goldup, N. Lebrasseur, D. A. Leigh. An autonomous chemically fuelled small-molecule motor, *Nature* **2016**, *534*, 235–240.

[15] C. Pezzato, C. Cheng, J. F. Stoddart, R. D. Astumian. Mastering the non-equilibrium assembly and operation of molecular machines, *Chem. Soc. Rev.* **2017**, *46*, 5491–5507.

[16] S. Kassem, T. Van Leeuwen, A. S. Lubbe, M. R. Wilson, B. L. Feringa, D. A. Leigh. Artificial molecular motors, *Chem. Soc. Rev.* **2017**, *46*, 2592–2621.

[17] S. Amano, S. D. P. Fielden, D. A. Leigh. A catalysis-driven artificial molecular pump, *Nature* **2021**, *594*, 529–534.

[18] S. Borsley, E. Kreidt, D. A. Leigh, B. M. W. Roberts. Autonomous fuelled directional rotation about a covalent single bond, *Nature* **2022**, *604*, 80–85.

[19] G. Ragazzon, L. J. Prins. Energy consumption in chemical fuel-driven self-assembly, *Nat. Nanotechnol.* **2018**, *13*, 882–889.

[20] E. Penocchio, R. Rao, M. Esposito. Thermodynamic efficiency in dissipative chemistry, *Nat. Commun.* **2019**, *10*, 3865.

[21] K. Das, L. Gabrielli, L. J. Prins. Chemically Fueled Self-Assembly in Biology and Chemistry, *Angew. Chem. Int. Ed.* **2021**, 2–26.

[22] A. Sharko, D. Livitz, S. De Piccoli, K. J. M. Bishop, T. M. Hermans. Insights into Chemically Fueled Supramolecular Polymers, *Chem. Rev.* **2022**, *122*, 11759–11777.

[23] M. Feng, M. K. Gilson. Enhanced Diffusion and Chemotaxis of Enzymes, *Annu. Rev. Biophys.* **2020**, *49*, 87–105.

[24] N. S. Mandal, A. Sen, R. D. Astumian. Kinetic Asymmetry versus Dissipation in the Evolution of Chemical Systems as Exemplified by Single Enzyme Chemotaxis, *J. Am. Chem. Soc.* **2023**, *145*, 5730–5738.

[25] N. S. Mandal, A. Sen, R. D. Astumian. A molecular origin of non-reciprocal interactions between interacting active catalysts, *Chem* **2023**, https://doi.org/10.1016/j.chempr.2023.11.017.

[26] T. Sangchai, S. Al Shehimy, E. Penocchio, G. Ragazzon. Artificial Molecular Ratchets: Tools Enabling Endergonic Processes, *Angew. Chem. Int. Ed.* **2023**, e202309501.

[27] S. Borsley, J. M. Gallagher, D. A. Leigh, B. M. W. Roberts. Ratcheting synthesis, *Nat. Rev. Chem.* **2023**, https://doi.org/10.1038/s41570-023-00558-y.

[28] R. D. Astumian. Irrelevance of the power stroke for the directionality, stopping force, and optimal efficiency of chemically driven molecular machines, *Biophys. J.* **2015**, *108*, 291–303.

[29] S. Amano, M. Esposito, E. Kreidt, D. A. Leigh, E. Penocchio, B. M. W. Roberts. Information thermodynamics of a synthetic molecular motor, *Nat. Chem.* **2022**, *14*, 530–537.

[30] E. Penocchio, G. Ragazzon. Kinetic Barrier Diagrams to Visualize and Engineer Molecular Nonequilibrium Systems, *Small* **2023**, 2206188.

[31] S. Corrà, M. T. Bakić, J. Groppi, M. Baroncini, S. Silvi, E. Penocchio, M. Esposito, A. Credi. Kinetic and energetic insights into the dissipative non-equilibrium operation of an autonomous light-powered supramolecular pump, *Nat. Nanotechnol.* **2022**, *17*, 746–751.

[32] L. Binks, S. Borsley, T. R. Gingrich, D. A. Leigh, E. Penocchio, B. M. W. Roberts. Chem, *Chem* **2023**, *9*, 2902–2917.

[33] G. Ragazzon, M. Malferrari, A. Arduini, A. Secchi, S. Rapino, S. Silvi, A. Credi. Autonomous Non-Equilibrium Self-Assembly and Molecular Movements Powered by Electrical Energy, *Angew. Chem. Int. Ed.* **2023**, *62*, e202214265.

[34] S. O. O. Krabbenborg, J. Veerbeek, J. Huskens. Spatially Controlled Out-of-Equilibrium Host-Guest System under Electrochemical Control, *Chem. Eur. J.* **2015**, *21*, 9638–9644.

[35] D. Barpuzary, P. J. Hurst, J. P. Patterson, Z. Guan. Waste-Free Fully Electrically Fueled Dissipative Self-Assembly System, *J. Am. Chem. Soc.* **2023**, *145*, 3727–3735.

[36] R. D. Astumian, I. Derényi. Fluctuation driven transport and models of molecular motors and pumps, *Eur. Biophys. J.* **1998**, *27*, 474–489.

[37] Koumura N., Zijlstra R.W.J., van Delden R. A., Harada N., Feringa B. L. Light-driven monodirectionalmolecular rotor, *Nature* **1999**, *401*, 152–154.

[38] V. Serreli, C.-F. Lee, E. R. Kay, D. A. Leigh. A molecular information ratchet, *Nature* **2007**, *445*, 523–527.

[39] G. Ragazzon, M. Baroncini, S. Silvi, M. Venturi, A. Credi. Light-powered autonomous and directional molecular motion of a dissipative self-assembling system, *Nat. Nanotechnol.* **2015**, *10*, 70–75.

[40] R. D. Astumian. Kinetic Asymmetry and Directionality of Nonequilibrium Molecular Systems, *Angew. Chem. Int. Ed.* **2023**, https://doi.org/10.1002/anie.202306569.

[41] A. J. Bard, L. R. Faulkner. Electrochemical Methods, *Electrochemical Methods*, John Wiley & Sons, **2001**.

[42] S. Erbas-Cakmak, D. A. Leigh, C. T. McTernan, A. L. Nussbaumer. Artificial Molecular Machines, *Chem. Rev.* **2015**, *115*, 10081–10206.

[43] S. Amano, M. Esposito, E. Kreidt, D. A. Leigh, E. Penocchio, B. M. W. Roberts. Using Catalysis to Drive Chemistry Away from Equilibrium: Relating Kinetic Asymmetry, Power Strokes, and the Curtin-Hammett Principle in Brownian Ratchets, *J. Am. Chem. Soc.* **2022**, *144*, 20153–20164.

[44] G. Falasco, T. Cossetto, E. Penocchio, M. Esposito. Negative differential response in chemical reactions, *New J. Phys.* **2019**, *21*, 073005.

[45] E. L. King, C. Altman. A schematic method of deriving the rate laws for enzyme-catalyzed reactions, *J. Phys. Chem.* **1956**, *60*, 1375–1378.

[46] T. L. Hill. Studies in irreversible thermodynamics IV. diagrammatic representation of steady state fluxes for unimolecular systems, *J. Theor. Biol.* **1966**, *10*, 442–459.
[47] K. M. Nam, R. Martinez-Corra, J. Gunawardena. The linear framework: Using graph theory to reveal the algebra and thermodynamics of biomolecular systems, *Interface Focus* **2022**, *12*, 20220013.
[48] T. L. Hill. Free Energy Transduction and Biochemical Cycle Kinetics, *Free Energy Transduction and Biochemical Cycle Kinetics*, Springer-Verlag, New York, **1989**.
[49] R. D. Astumian, B. Robertson. Imposed oscillations of kinetic barriers can cause an enzyme to drive a chemical reaction away from equilibrium, *J. Am. Chem. Soc.* **1993**, *115*, 11063–11068.
[50] R. D. Astumian. Trajectory and Cycle-Based Thermodynamics and Kinetics of Molecular Machines: The Importance of Microscopic Reversibility, *Acc. Chem. Res.* **2018**, *51*, 2653–2661.
[51] M. Shetty, A. Walton, S. R. Gathmann, M. A. Ardagh, J. Gopeesingh, J. Resasco, T. Birol, Q. Zhang, M. Tsapatsis, D. G. Vlachos, P. Christopher, C. D. Frisbie, O. A. Abdelrahman, P. J. Dauenhauer. The Catalytic Mechanics of Dynamic Surfaces: Stimulating Methods for Promoting Catalytic Resonance, *ACS Catal.* **2020**, *10*, 12666–12695.
[52] A. Sabatino, E. Penocchio, G. Ragazzon, A. Credi, D. Frezzato. Individual-Molecule Perspective Analysis of Chemical Reaction Networks: The Case of a Light-Driven Supramolecular Pump, *Angew. Chem. Int. Ed.* **2019**, *58*, 14341–14348.
[53] X. Zhao, H. Palacci, V. Yadav, M. M. Spiering, M. K. Gilson, P. J. Butler, H. Hess, S. J. Benkovic, A. Sen. Substrate-driven chemotactic assembly in an enzyme cascade, *Nat. Chem.* **2018**, *10*, 311–317.
[54] L. J. Prins, F. Ricci, et al. -, **2024**, in preparation.
[55] T. Marchetti, B. M. W. Roberts, D. Frezzato, L. J. Prins. A minimalistic synthetic metabolic cycle that consumes ADP, *submitted* **2024**.
[56] J. Leira-Iglesias, A. Tassoni, T. Adachi, M. Stich, T. M. Hermans. Oscillations, travelling fronts and patterns in a supramolecular system, *Nat. Nanotechnol.* **2018**, *13*, 1021–1028.
[57] E. Del Grosso, I. Ponzo, G. Ragazzon, L. J. Prins, F. Ricci. Disulfide-Linked Allosteric Modulators for Multi-cycle Kinetic Control of DNA-Based Nanodevices, *Angew. Chem. Int. Ed.* **2020**, *59*, 21058–21063.
[58] M. G. Howlett, A. H. J. Engwerda, R. J. H. Scanes, S. P. Fletcher. An autonomously oscillating supramolecular self-replicator, *Nat. Chem.* **2022**, *14*, 805–810.
[59] S. Gentile, E. Del Grosso, L. J. Prins, F. Ricci. Autonomous and Programmable Reorganization of DNA-Based Polymers Using Redox Chemistry**, *Chem. Eur. J.* **2023**, *29*, e202300394.
[60] C. Pezzato, M. T. Nguyen, D. J. Kim, O. Anamimoghadam, L. Mosca, J. F. Stoddart. Controlling Dual Molecular Pumps Electrochemically, *Angew. Chem. Int. Ed.* **2018**, *57*, 9325–9329.
[61] L. Zhang, Y. Qiu, W. G. Liu, H. Chen, D. Shen, B. Song, K. Cai, H. Wu, Y. Jiao, Y. Feng, J. S. W. Seale, C. Pezzato, J. Tian, Y. Tan, X. Y. Chen, Q. H. Guo, C. L. Stern, D. Philp, R. D. Astumian, W. A. Goddard, J. F. Stoddart. An electric molecular motor, *Nature* **2023**, *613*, 280–286.
[62] S. Borsley, M. M. Haugland, S. Oldknow, J. A. Cooper, M. J. Burke, A. Scott, W. Grantham, J. Vallejo, E. K. Brechin, P. J. Lusby, S. L. Cockroft. Electrostatic Forces in Field-Perturbed Equilibria: Nanopore Analysis of Cage Complexes, *Chem* **2019**, *5*, 1275–1292.
[63] Y. Zhang, H. Hess. Chemically-powered swimming and diffusion in the microscopic world, *Nat. Rev. Chem.* **2021**, *5*, 500–510.
[64] S. Borsley. Membrane Transport, Molecular Machines, and Maxwell's Demon, *ChemSystemsChem* **2024**, e202400004.
[65] E. Branscomb, T. Biancalani, N. Goldenfeld, M. Russell. Escapement mechanisms and the conversion of disequilibria; the engines of creation, *Phys. Rep.* **2017**, *677*, 1–60.
[66] A. Ianeselli, A. Salditt, C. Mast, B. Ercolano, C. L. Kufner, B. Scheu, D. Braun. Physical non-equilibria for prebiotic nucleic acid chemistry, *Nat. Rev. Phys.* **2023**, *5*, 185–195.
[67] K. B. Muchowska, S. J. Varma, J. Moran. Nonenzymatic Metabolic Reactions and Life's Origins, *Chem. Rev.* **2020**, *120*, 7708–7744.
[68] E. Moulin, L. Faour, C. C. Carmona-vargas, N. Giuseppone. From Molecular Machines to Stimuli-Responsive Materials, *Adv. Mater.* **2019**, 1906036.
[69] O. E. Shklyaev, A. C. Balazs. Interlinking spatial dimensions and kinetic processes in dissipative materials to create synthetic systems with lifelike functionality, *Nat. Nanotechnol.* **2023**, https://doi.org/10.1038/s41565-023-01530-z.
[70] H. Zhou, T. Yamada, N. Kimizuka. Supramolecular Thermo-Electrochemical Cells: Enhanced Thermoelectric Performance by Host-Guest Complexation and Salt-Induced Crystallization, *J. Am. Chem. Soc.* **2016**, *138*, 10502–10507.
[71] S. Di Noja, M. Garrido, L. Gualandi, G. Ragazzon. Control over Dethreading Kinetics Allows Evaluating the Entropy Stored in an Interlocked Molecular Machine Out-of-Equilibrium, *Chem. Eur. J.* **2023**, *29*, e202300295.
[72] Y. Tu. The nonequilibrium mechanism for ultrasensitivity in a biological switch: Sensing by Maxwell's demons, *Proc. Natl. Acad. Sci. U. S. A.* **2008**, *105*, 11737–11741.
[73] S. O. Krabbenborg, J. Huskens. Electrochemically generated gradients, *Angew. Chem. Int. Ed.* **2014**, *53*, 9152–9167.